Electrochemical corrosion behavior of plasma sprayed Cr_2O_3-25TiO_2 composite coatings

Q. H. Song[a], F. S. Hao[b], Y. F. Zhang[a,*], Q. Li[c], J. J. Li[a]
[a]*School of Mechanical & Automotive Engineering, Qilu University of Technology (Shandong Academy of Sciences), Jinan, Shandong, 250353, PR China*
[b]*Weihai Yinxing Prestressed Wire Products Co.,Ltd, Weihai, Shandong, 264200, PR China*
[c]*School of Material Science & Engineering, Qilu University of Technology, Shandong Academy of Sciences, Jinan, Shandong, 250353, PR China*

In this paper, Cr_2O_3-25TiO_2 composite coatings were prepared on the surface of steel structure samples by atmospheric plasma spraying. The phase composition, microstructure, microhardness and long-term immersion corrosion behavior in 3.5 wt.% NaCl solution of Cr_2O_3-25TiO_2 composite coatings were studied. The corrosion behavior of Cr_2O_3-25TiO_2 composite coating was analyzed by potentiodynamic polarization and electrochemical impedance spectroscopy. The impedance data were fitted into an appropriate equivalent circuit to explain the electrochemical corrosion behavior of the coating at different stages. The results of scanning electron microscopy showed that the Cr_2O_3-25TiO_2 composite coating was agglomerated, and the rhombohedral Cr_2O_3 powder was wrapped around the rhombohedral TiO_2 powder. The coating melted completely without obvious defected. The XRD results showed that no phase transformation occurred in the Cr_2O_3-25TiO_2 composite coating. The Cr_2O_3-25TiO_2 coatings showed high corrosion resistance and good passivation behavior in the initial stage of corrosion. The coating itself did not corrode. With the extension of corrosion time, the corrosive medium had passed through the pores between the coatings, resulting in the contact between the corrosive medium and the matrix interface, resulting in the matrix corrosion damage. Corrosion products would deposit on the surface of the coating, blocking the pores between the coatings, and the corrosion rate would be reduced.

(Received March 17, 2023; Accepted June 9, 2023)

Keywords: Plasma spraying, Cr_2O_3-25TiO_2 coating, Microstructure, Electrochemical corrosion

1. Introduction

Corrosion was an inevitable problem that affected the service life of the material, resulting in a decrease in the intermittent strength of the coating and a rapid peeling of the coating, which

* Corresponding author: zhangyanfei@qlu.edu.cn
https://doi.org/10.15251/DJNB.2023.182.751

ultimately leaded to coating failure and damaged to the substrate [1]. Thermal spraying technology was one of the widely used surface treatment technologies. It was mainly used to prepare anti-corrosion and wear-resistant coatings for steel structures. Compared with other spraying technologies, it had the advantages of convenient use, low energy consumption, high bonding strength and low porosity. In the case of plasma spraying, the plasma was generated by the arc combustion in the plasma gun nozzle, and the arc gas formed a plasma jet when it flowed out of the nozzle. The powder particles were injected into the plasma jet and then hit the surface, creating an adherent coating. The plasma spraying technology was stable, and the ceramic coating with dense structure and stable performance could be obtained. The plasma spraying technology was used to combine the toughness of metal materials with the advantages of corrosion resistance, wear resistance, high hardness, strong thermal insulation, low linear expansion coefficient and no pollution of ceramic materials, which could meet the use of equipment and its components under harsh conditions [2]. Cr_2O_3 ceramics with high hardness and small friction coefficient were very good wear-resistant coating materials. However, Cr_2O_3 ceramics were brittle and brittle when sprayed. Adding a certain amount of TiO_2 to Cr_2O_3 could significantly improve the deposition efficiency of the powder and the wear resistance of the coating [3,4]. Moreover, it could enhance the toughness of the composite coating, maintained the high hardness of the coating, reduced the tendency of cracking in the process of spraying, so that it had the smallest structural defects [5]. Cr_2O_3-TiO_2 coating had high hardness and high temperature stability, excellent wear resistance, corrosion resistance and heat resistance, and was widely used in the wear resistance and corrosion resistance of Auxin round shaft [6].

Nan-nan Li et al. [7] prepared Cr_2O_3-TiO_2 composite powders with different contents of TiO_2 on the surface of stainless steel by plasma spraying, and studied the microstructure and wear resistance of the coating. The results showed that the addition of TiO_2 could significantly reduce the cracking trend of the coating. With the increase of TiO_2 content, the porosity of the coating increased first and then decreased, and the friction coefficient of the coating decreased continuously. Sreenivas Rao K V et al. [8] characterized the corrosion behavior of Cr_2O_3-Al_2O_3-ZrO_2 coating by salt spray test. The results showed that the surface of Cr_2O_3-Al_2O_3-ZrO_2 multilayer coated steel had better corrosion resistance than that of uncoated steel at higher exposure time due to its higher microhardness and better chemical resistance. Aishwarika Raj Sharma et al. [9] studied the corrosion behavior of Al_2O_3-13 wt.% TiO_2 and Cr_2O_3 coatings in artificial seawater environment by immersion test and weight measurement. The results showed that the corrosion of Cr_2O_3 coating was the smallest after 55 days of immersion, and the maximum corrosion was deposited on the surface of hull steel, and the rust color was reddish brown. The corrosion resistance of chromium oxide coating was greater than that of composite coating.

In this paper, the microstructure of plasma sprayed Cr_2O_3-25TiO_2 composite coating and its immersion corrosion behavior in 3.5 wt.% NaCl were studied. The long-term protection performance of plasma sprayed Cr_2O_3-25TiO_2 composite coatings in 3.5 wt.% NaCl solution was investigated by electrochemical impedance spectroscopy (EIS) at different immersion time.

2. Material and methods

2.1. Preparation of the coating

In this study, Cr_2O_3-25TiO_2 composite powder with particle size range of 15-45μm and Ni-Al powder with particle size range of 180-325 mesh produced by Jinzhou Jinjiang Company were used. The substrate material was 304 steel sheet, the specification was 13mm × 10mm × 2mm. Before spraying, the steel sample was sandblasted with white corundum under air pressure of 0.79 MPa. The purpose of sandblasting was to remove impurities from the surface of the material while increasing the surface roughness so that the coating could form a good mechanical bonding with the substrate. After sand blasting, ZB-800 plasma spraying power supply and HV-80-JP powder feeder (Zhengzhou Lijia) produced by Beijing Aerospace Zhenbang Company were used for spraying. ZYH-20 (Jintai Welding) was used as powder drying furnace, and argon and hydrogen were used as main gas and secondary gas respectively [10]. The detailed spraying process parameters were shown in Table 1, and the final coating thickness was 122μm. The whole spraying process was carried out indoors to prevent excessive oxidation during coating formation. After spraying, the sample was air-cooled to room temperature to prevent greater internal stress between the coatings. After the sample collection, the sample was further analyzed.

Table 1. Spray parameters for the APS process.

Powder	Ni-Al	Cr_2O_3-25TiO_2
Current (A)	630	633
Voltage (V)	65	72
Primary plasma gas; Ar(l/min)	34	34
Secondary plasma gas; H_2 (l/min)	3	3
Powder feed air flow rate (NLPM)	4.7	8
Spray distance (mm)	140	140

2.2. Characterization

The coating samples were qualitatively analyzed on a D8-ADVANCE (Germany) X-ray diffractometer (XRD) using a continuous scanning with a scanning speed of 20 °/min and a scanning range of 10°-90°. In order to observe the microstructure, the coating was inlaid with epoxy resin. After the resin was hardened, the samples were ground with 400 #, 600 # and 800 # SiC sandpaper respectively, and polished with a universal metallographic sample polishing machine (HYP-1). The morphology and microstructure of the coatings were characterized by an ultra-high resolution scanning electron microscope (SEM, GeminiSEM 500, Carl Zeiss, Germany).

The microhardness of the coating was measured by HXD-1000TMC micro Vickers hardness tester. The test load was set at 200 g, the loading time was set at 15 s, and 6 points were measured and averaged. The SF200 surface roughness tester was used to test the surface roughness of the coating, and the average value was measured 5 times continuously. Electrochemical tests were performed at room temperature using an Interface1000 electrochemical workstation. Three electrode system was adopted: the working electrode was a sample with an exposure area of about 1cm^2; The reference electrode was saturated calomel electrode (SCE); The auxiliary electrode was

a large area platinum plate electrode. The corrosive medium was 3.5 wt.% (mass fraction) NaCl solution, prepared with primary distilled water, and the reagent was analytically pure. The scanning range was -0.25 ~ 1V, and the scanning speed was 0.5 mV/s. The initial stabilization time of the test was 3600 s, and it was tested after the open circuit potential was stabilized. The electrochemical impedance data were fitted and analyzed by Zsimpwin software.

3. Results and discussion

3.1. Coating characterization

Figure 1 showed the XRD patterns of the Cr_2O_3-25TiO_2 coating and powder, as well as a PDF card for reference. It could be seen that both the powder and the coating contained Cr_2O_3 and TiO_2 phases, and no diffraction peaks of other phases were found. The phase composition of the powder and the coating changed little, and the diffraction peaks did not shift in a large range, indicating that the material did not undergo large lattice expansion or contraction. Due to the characteristics of Cr_2O_3 material, the crystal had a high melting point and the diffraction peaks of the stable powder and the coating corresponded to each other, and no new diffraction peaks appeared, indicating that in the process of preparing the coating, the material did not undergo phase transition and serious expansion and contraction. The product was only the mechanical mixing of the reactants and the structure was stable.

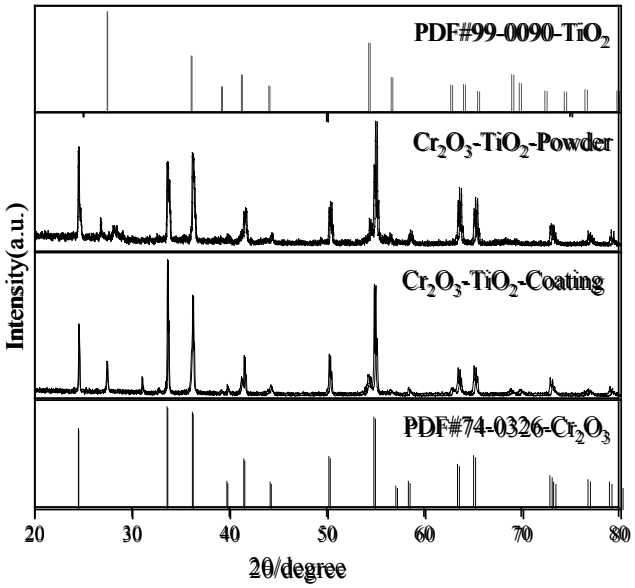

Fig. 1. XRD pattern of the Cr_2O_3-25TiO_2 coating and powder.

Figure 2 showed the surface morphology of Cr_2O_3-25TiO_2 composite powder. It could be seen that rhombic hexahedral Cr_2O_3 powder was wrapped around rhombohedral TiO_2 powder, showing a agglomerated distribution [11]. The agglomerated powder was ellipsoidal, the powder surface was dense and smooth, and the powder had good fluidity, which could meet the requirements of plasma spraying.

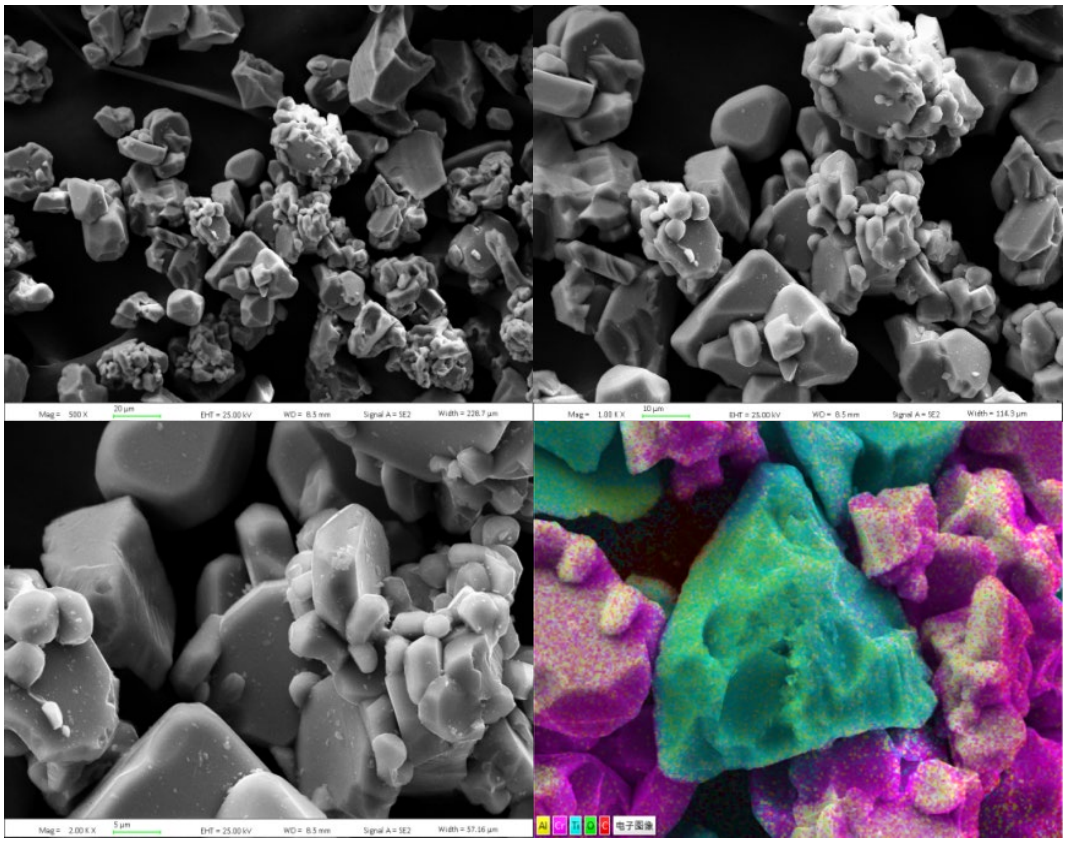

Fig. 2. SEM micrographs of Cr_2O_3-25TiO_2 powder

Figure 3 showed the surface morphology of the of Cr_2O_3-25TiO_2 coating. The preparation of the coating was that the composite powder was heated to the melting state by plasma arc, which was accelerated and stacked with each other, and continuously enriched on the surface of the substrate to form the coating, so that the coating had a layered microstructure [12]. The surface structure of the coating was complex, and there were many irregular protrusions on the surface. Because the powder particles were not completely formed by melting, and the unmelted particles are embedded between the molten particles and wrapped layer by layer. The existence of fine cracks in the box was due to the quenching stress and thermal mismatch stress generated when the ceramic powder was heated to the molten state and the droplet solidified and shrinked. The formation of pores was caused by impurities in the spraying environment on the one hand. On the other hand, it was due to the incomplete melting of the powder during the spraying process. Figure 3d showed the EDS element mapping of the coating. Parts A and B were TiO_2 rich areas and Cr_2O_3 rich areas, respectively, and TiO_2 was fully melted and fully spread out. Cr_2O_3 adsorbed near TiO_2, rough surface, poor deposition, coating structure fluffy and pits. The reason for enrichment might be that the melting point of TiO_2 was lower than that of Cr_2O_3, and TiO_2 had a certain adsorption after melting, forming a solid solution structure. On the whole, the coating melts completely and the structure was dense, which was beneficial to improve the hardness and corrosion resistance of the coating.

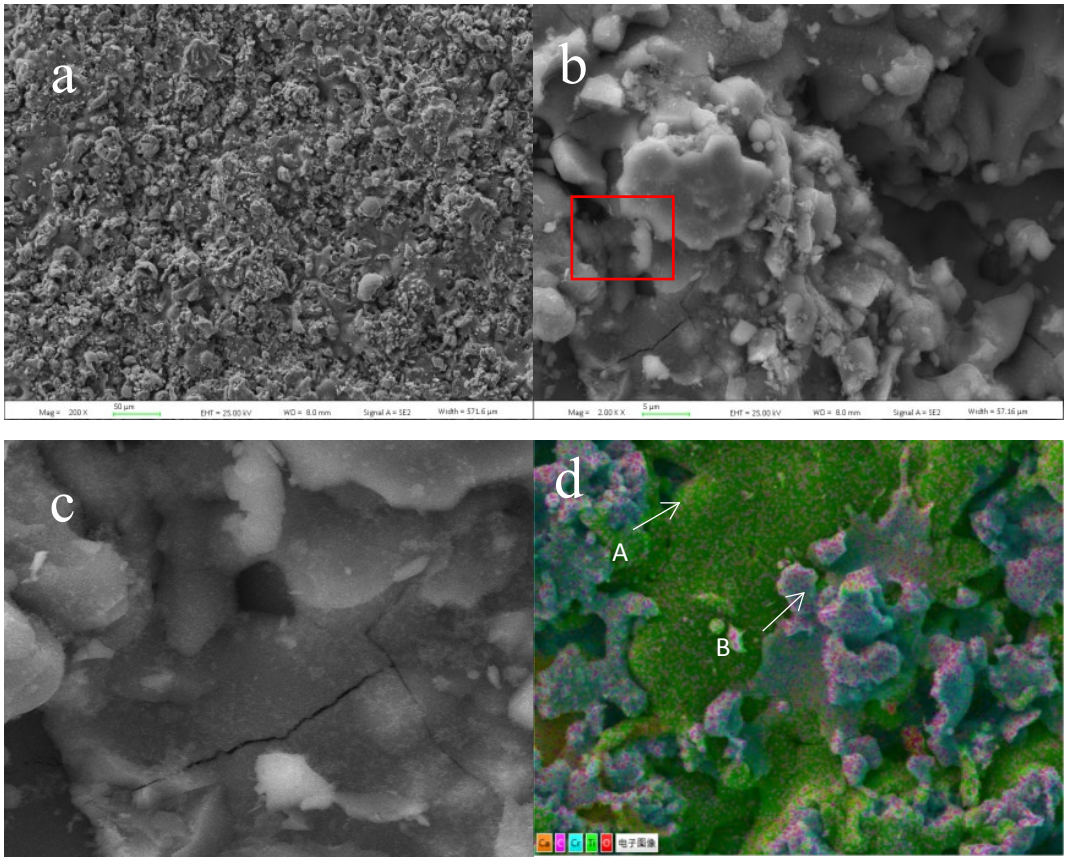

Fig. 3. SEM micrographs of Cr_2O_3-25TiO_2 coating

3.2. Microhardness of coating

Hardness was an important parameter determining the performance of plasma sprayed coating system [13]. Figure 4 showed the microhardness test results of the two coatings. The hardness of Cr_2O_3-25TiO_2 coating changed greatly, the maximum was 802 $HV_{0.2}$, the minimum was 633.7 $HV_{0.2}$, and the average hardness was 702.85 $HV_{0.2}$. This was related to the compactness and oxidation of the coating. In the experiment, near the adhesive layer, the hardness value was low, and near the surface side, the average hardness value of more than 800$HV_{0.2}$. In the process of coating formation, the temperature after spraying reached more than 600 °C. In order to reduce the internal stress between the coatings, it was necessary to continue spraying after cooling to below 80 °C. The reason for the low hardness near the bonding layer might be that the temperature was too high during the spraying process, the Cr_2O_3-25TiO_2 coating had a small amount of oxidation, and the pores were relatively increased.

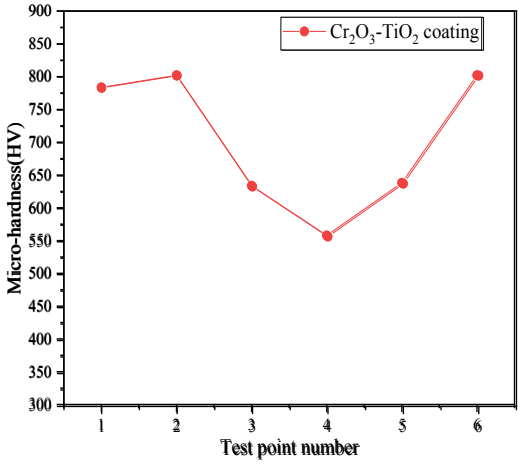

Fig. 4. Microhardness test results

3.2. Corrosion performance of the coating

3.2.1. Tafel curve test

Figure 5 showed the potentiodynamic polarization curve of plasma sprayed Cr_2O_3-25TiO_2 coating and matrix sample in 3.5 wt.% NaCl solution. The values of corrosion potential (E_{corr}), corrosion current density (I_{corr}) and Tafel slope (β_a, β_c) were extracted from the curves by Tafel extrapolation, as shown in Table 2. The self-corrosion potential of Cr_2O_3-TiO_2 coating was slightly lower than that of the substrate, indicating that the corrosion tendency of Cr_2O_3-TiO_2 coating was greater than that of the substrate at the initial stage of corrosion. Cr_2O_3-TiO_2 coatings showed obvious passivation behavior, and the passivation of Cr_2O_3-TiO_2 coatings was related to the formation of TiO_2 surface film. After the polarization curve, no precipitation product was observed in the corrosion solution, and the corrosion medium was difficult to erode after the coating was passivated. The corrosion resistance of the coating was affected by the oxide content. Corrosion could preferentially start at the boundary between particles, possibly due to micro-galvanic corrosion. Therefore, the solution penetrated the boundary between the particles and reached the substrate.

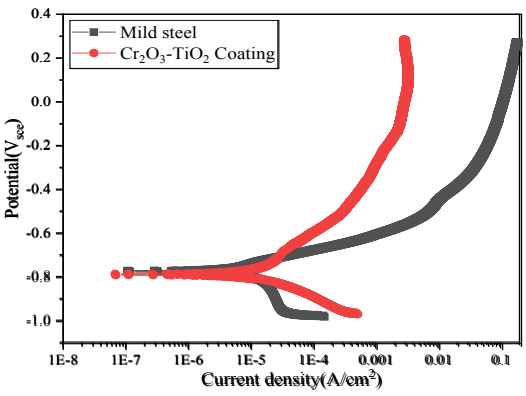

Fig. 5. Polarization curve of Cr_2O_3-25TiO_2 coating

Table 2. Electrochemical parameter of Cr_2O_3-25TiO_2 coating were extracted from potentiodynamic polarization curves in 3.5 wt.% NaCl solution.

Sample	E_{corr}/V	I_{corr}/A·cm^{-2}	β_a	β_c
Steel substrate	-0.76589	2.2516×10^{-5}	61.036	148.65
Cr_2O_3-25TiO_2 coating	-0.78078	4.077×10^{-6}	107.23	81.291

3.2.2. EIS analysis of coating corrosion failure process

Figure 6 was the electrochemical impedance spectroscopy of Cr_2O_3-25TiO_2 samples immersed in 3.5 wt.% NaCl solution for different time. At the beginning of soaking, the coating surface was smooth without corrosion products. Within 2 days of immersion, the curve in the Nyquist diagram contained two arcs, and the Bode diagram contained two inflection points, indicating that there were two time parameters at this time, which were high frequency capacitance loop and low frequency capacitance loop. The high frequency capacitive loop corresponded to the corrosion product capacitance and corrosion product resistance, and the low frequency capacitive loop corresponded to the double layer capacitance and charged transfer resistance. Since the thermal spray coating was affected by the process, there were pores between the coatings, as reflected in the Nyqusit diagram with two semicircles [14]. In the early stage of immersion, the coating played a blocking role, the corrosive medium entered the pores of the coating surface, but did not reach the depth of the coating, and the surface corrosion pore size was small, the corrosion rate was slow [15,16]. Due to the density, low porosity and stable chemical properties, the coating formed an oxide film after 12h immersion to prevent further entry of corrosive media. The corrosion medium that had entered the pores of the coating was difficult to diffuse out, and the corrosion products were adhered to the pores, so that the inside of the gap could not be smoothly exchanged with the corrosion medium. At this time, the coating impedance value increased. The semicircle radius of the corresponding Nyquist diagram increased, and the semicircle radius reached the maximum after soaking for 1d. It could be seen from the data in Table 3 that the value of R_t increased from 847Ω·cm^2 to 6018Ω·cm^2 after soaking for 0h-2d. The value of n was also increasing, and the dispersion coefficient n represented the uniformity of the capacitance surface. The n represented the density and uniformity of the coating surface. At this time, it could be explained that the irregular points in the coating surface were corroded within 2 days of immersion, the overall coating surface was smoother than that after spraying, and the corrosion products gradually accumulated on the coating surface. The phase angle value in the Bode diagram increased first and then decreased. The equivalent circuit of the electrode system at this stage fitted by software was R(Q(R(CR))), as shown in Figure 8. R_1 was the solution resistance; Q_c was the constant phase angle element of the coating surface/dielectric interface, usually denoted by Y_0 and n. When n=0 represented pure resistance, n=1 represented pure capacitance. $R_{1,\,p1}$ represented the surface pore resistance in the pores of the coating, and R_t represented the charge transfer resistance. After 6 days of immersion, more corrosion products were deposited on the surface of the coating, which made it impossible for the corrosion products inside the coating to diffuse. At this time, the pure capacitance C_v inside the coating was replaced by the constant phase angle element Q_v of the coating/medium interface dispersion effect. The electrode system fitting circuit corresponding to this stage was R(Q(R(QR))), as shown in Figure 9.

When the corrosion time to 12d, the coating surface pores gradually increased, the gas generated inside the pores and the external pressure difference, resulting in the diffusion of corrosion products, corrosion medium could be completed in the coating pores exchange. At this time, some of the holes reached the steel matrix and caused some damage to the matrix. The equivalent circuit of the electrode system was R(C(R(Q(R(CR))))). Qv represented the constant phase angle element between the metal/medium inside the pitting hole on the coating surface, and C_a represented the capacitance of the metal-medium interface where sacrificial anodic dissolution occurred in the pitting hole deep into the substrate. $R_{1, p2}$ represented the pore resistance deep into the coating.

As the corrosion medium penetrated into the coating, the phase angle decreased in the medium frequency and low frequency range, which was due to the formation of conductive percolation channels in the coating. The phase angle of the coating did not decrease at low frequency, indicating that it had good corrosion resistance. With the increase of immersion time, the surface pore resistance $R_{1, p1}$ in the coating pores gradually decreased. After 12 days, the pore resistance $R_{1, p1}$ on the coating surface decreased from 1.705Ω·cm^2 to 0.8906Ω·cm^2 when the corrosive medium reached the matrix interface. The corrosive medium had penetrated into the interior of the coating, and the surface resistance had basically failed. And the Q_a-Y_0 value of the constant phase angle element at the coating depth/substrate interface decreased. The equivalent circuit of the corresponding electrode system was R(C(R(Q(R(QR))))). Since the capacitance value was proportional to the dielectric constant and surface area, it was proportional to the distance between the two layers of capacitance. When the surface of the sprayed coating was covered with corrosion products, the dielectric constant of the capacitor decreased. After immersion for 30 days, the corrosion products near the substrate gradually increased, the corrosion medium corroded the substrate, and the coating gradually lost its corrosion resistance.

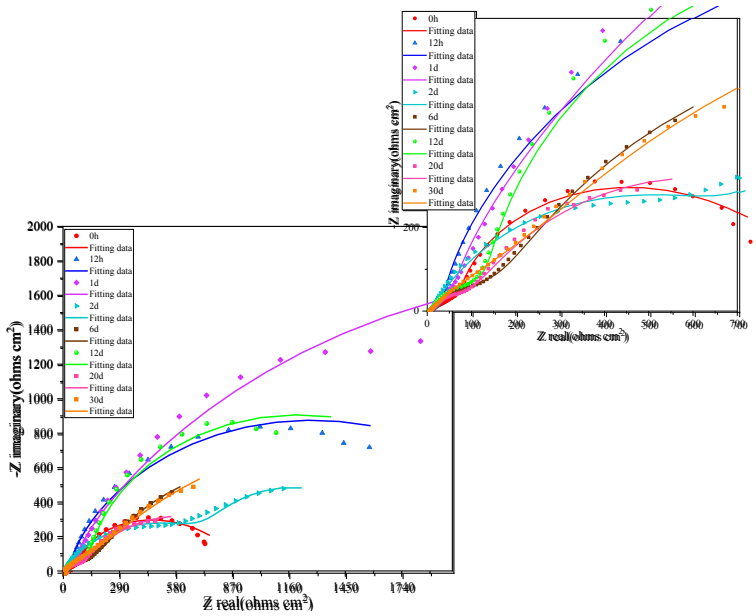

Fig. 6. Nyquist diagram of Cr_2O_3-25TiO_2 coating with different immersion time

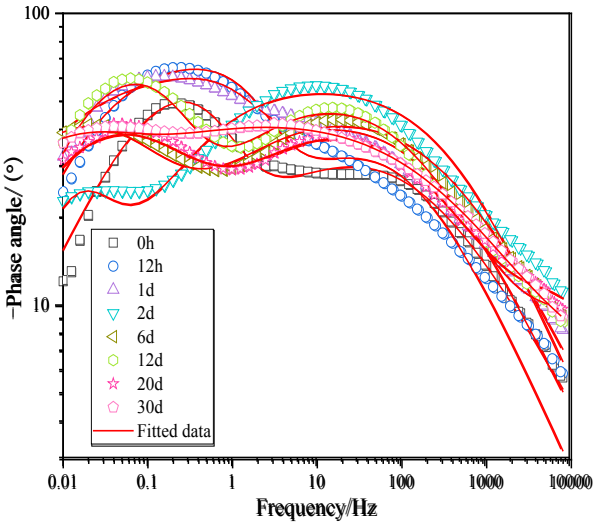

Fig. 7. Frequency-phase angle of Cr_2O_3-25TiO_2 coating with different immersion time

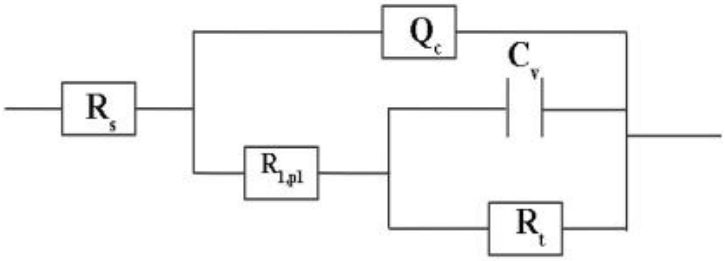

Fig. 8. EIS Equivalent Circuit Model R(Q(R(CR))).

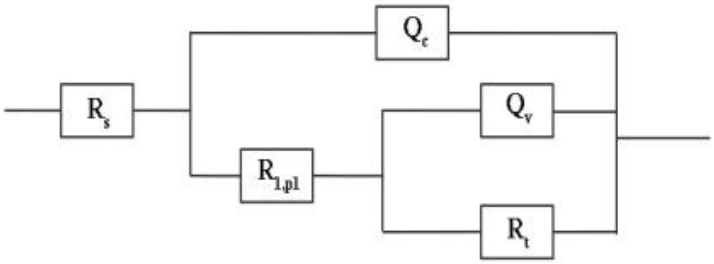

Fig. 9. EIS Equivalent Circuit Model R(Q(R(QR)))

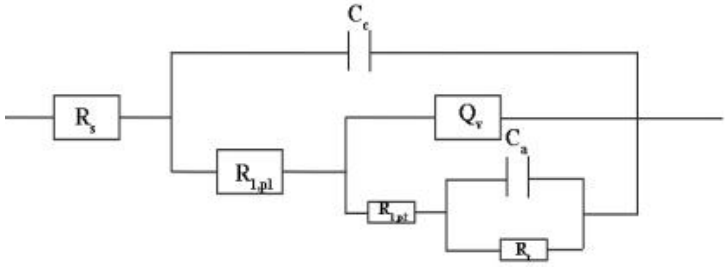

Fig. 10. EIS Equivalent Circuit Model R(C(R(Q(R(CR))))).

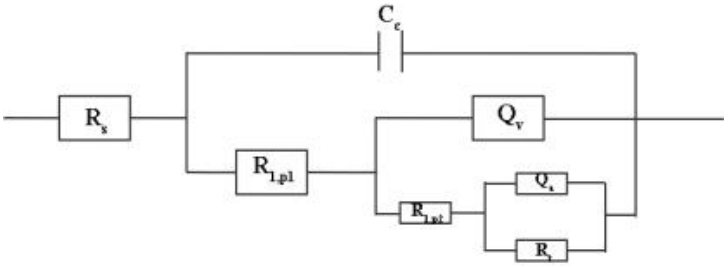

Fig. 11. EIS Equivalent Circuit Model R(C(R(Q(R(QR)))))

Table 3. Impedance spectrum fitting results of Cr_2O_3-25TiO_2 coating in 3.5 wt.% NaCl.

Immersion time	0h	12h	1d	2d	6d	12d	20d	30d
$R_s/(\Omega \cdot cm^2)$	10.18	7.704	6.681	6.579	5.646	5.263	6.025	5.369
Q_c-Y_0	0.001603	0.001467	0.001519	0.0007085	0.001537	-	-	-
n_1	0.57	0.6628	0.6283	0.6788	0.602	-	-	-
C_c	-	-	-	-	-	9.324E-006	7.825E-006	4.548E-006
$R_{1, p1}$	110.5	56.98	162	916.1	220.7	1.705	2.14	0.8906
Q_v-Y_0	-	-	-	-	0.007195	0.001269	0.001669	0.003069
n_2	-	-	-	-	0.7331	0.6685	0.6140	0.5227
C_v	0.001894	0.001061	0.0005354	0.01589	-	-	-	-
$R_{1, p2}$	-	-	-	-	-	224.5	139.2	846.3
Q_a-Y_0	-	-	-	-	-	-	0.006356	0.003248
n_3	-	-	-	-	-	-	0.7214	0.7437
C_a	-	-	-	-	-	0.003126	-	-
R_t	847	2604	6018	815.7	1999	2236	994.6	2551

Figure 12 showed the surface micro morphology and EDS element mapping of Cr_2O_3-25TiO_2 coating after different immersion times. The surface of the coating was smooth and flat within 6 days of immersion, and the coating was layered on the surface of the substrate. After 6 days of immersion, the surface of the coating showed a tendency to corrode, and a small amount of micropores and cracks appeared on the surface of the completely melted coating. At this time, a small amount of C element appeared on the surface, indicating that the corrosive medium had reached the matrix interface and eroded the matrix. After 20 days of immersion, the coating surface O and Fe elements increased significantly. A large number of substances appeared on the surface of the coating adsorbed on the surface of the coating. After soaking for 30 days, the overall coating was honeycomb, and micro-cracks appeared on the surface of the coating. The coating

could still combine well with the substrate to provide protection for the substrate. From the perspective of the corrosion process, the coating provided a barrier for the substrate. Due to the presence of Cr element, the coating itself was difficult to corrode. In the Cr element-rich area, although it was soaked for 30 days, it was difficult to find the presence of Fe element and its oxides around. Ceramic coatings themselves were difficult to corrode, but corrosion solutions could penetrate through pores and cracks [17]. The main reason for the corrosion of the substrate was that there were pores in the middle of the coating during the spraying process, and these pores were difficult to avoid. The corrosive medium reached the substrate interface through the pores between the coatings, causing corrosion damage to the substrate. Therefore, it was necessary to reduce the coating porosity, as far as possible from the spraying parameters, spraying environment and post-treatment three aspects to solve the problem of coating porosity.

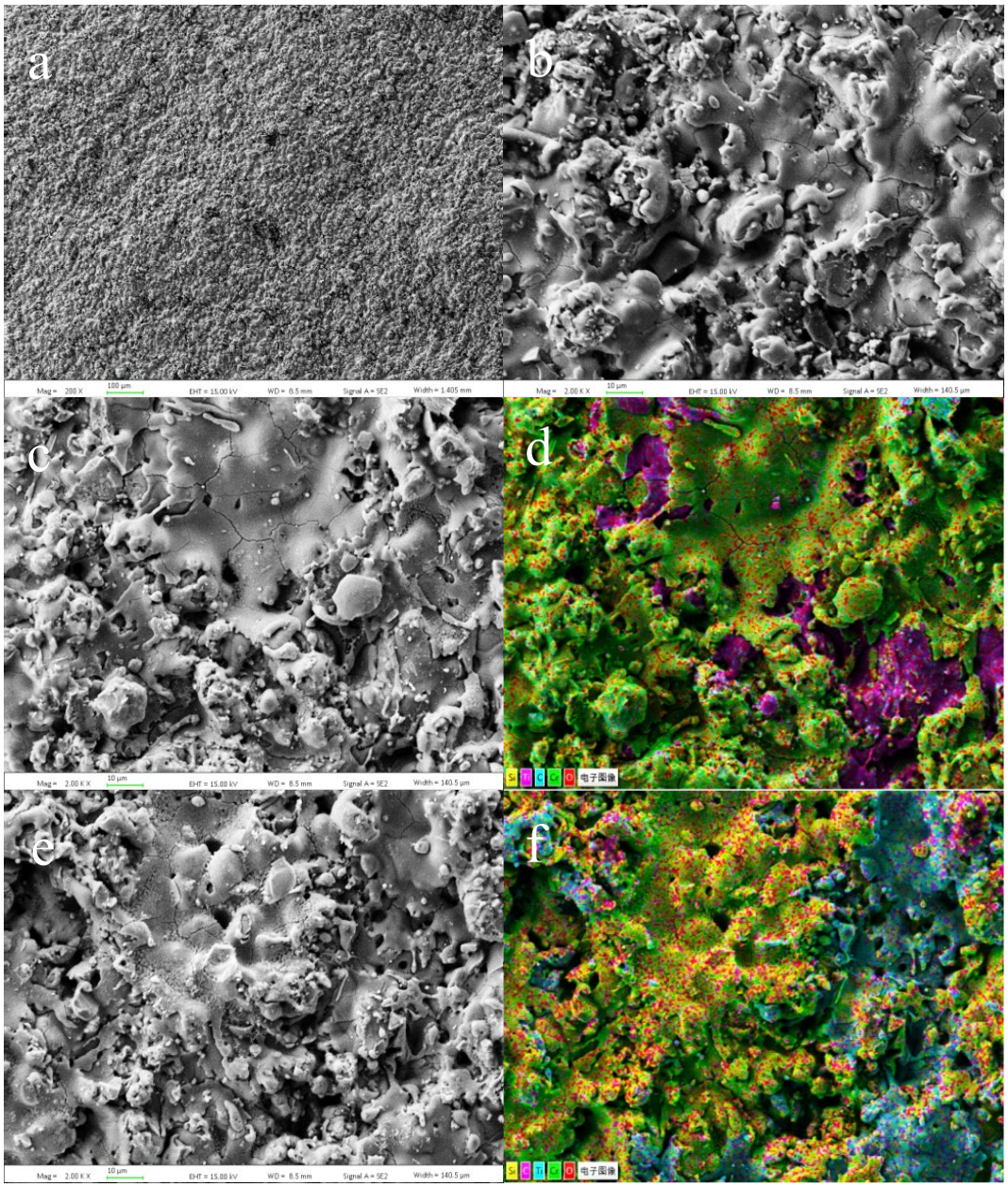

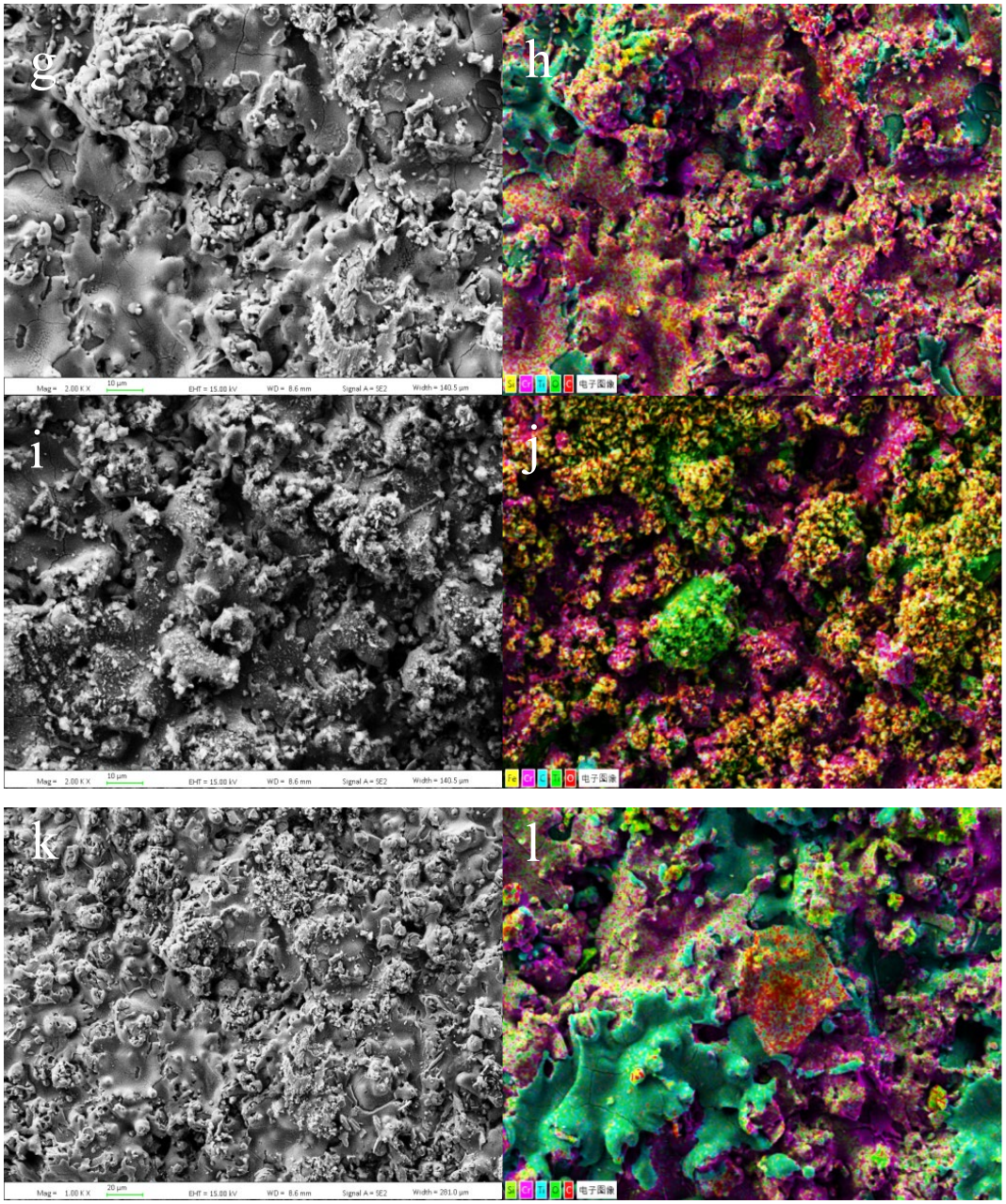

Fig. 12. Surface morphology of the coating after different immersion time and EDS element mapping diagram (a-b) Corrosion 1 day (c-d) Corrosion 2 days (e-f) Corrosion 6 days (g-h) Corrosion 12 days (i-j) Corrosion 20 days (k-l) Corrosion 30 days.

Figure 13 showed the X-ray diffraction of Cr_2O_3-25TiO_2 coating after 30 days of immersion. The surface was mainly Cr_2O_3 phase and a small amount of NaCl. The phase of the coating did not change greatly after 30 days of immersion, indicating that the coating had very good corrosion resistance. There were a lot of reddison-brown flocculent substances in the soaking solution, and the corrosive medium had passed through the pores of the coating to the matrix, resulting in certain corrosion on the matrix interface.

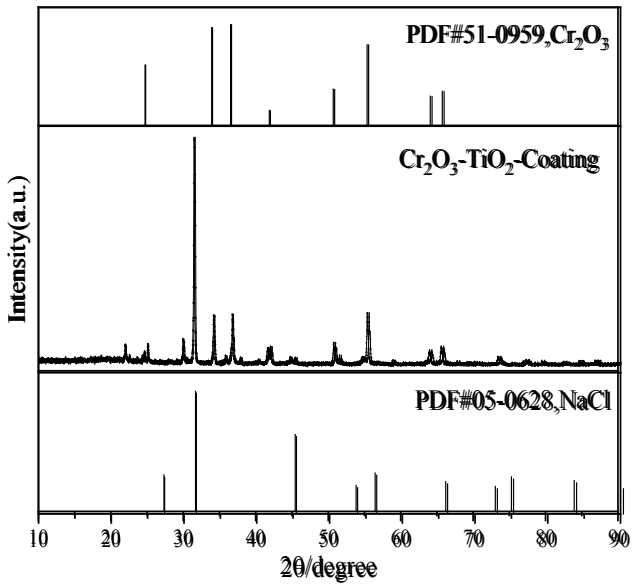

Fig. 13. XRD pattern of Cr_2O_3-25TiO_2 coating after immersion for 30 days

4. Conclusion

Cr_2O_3-25TiO_2 coating was prepared on steel substrate by plasma spraying, and the microstructure and corrosion resistance of the coating were analyzed. The average hardness of the coating was 702.85 $HV_{0.2}$, and the surface was typical layered structure. The polarization results showed that the Cr_2O_3-25TiO_2 coating had a lower self-corrosion potential than the substrate, and the corrosion rate was slightly higher than the substrate. The coating had good passivation behavior, and its main function was to provide barrier protection for the substrate. Based on the EIS results, some equivalent circuits were established to explain the electrochemical corrosion behavior of the coating. In the early stage of immersion, the corrosion resistance of the coating showed an increasing trend, and the corrosion resistance was the best when immersed for 1 day. With the increase of immersion time, the corrosive medium reached the substrate interface through the pores between the coatings, resulting in corrosion of the substrate. After 30 days of immersion, the surface of the coating was honeycomb-like, C element was found at the pore defects of the coating, and cracks appeared in some molten areas. The coating had no shedding and peeling as a whole, and could still provide good protection for the substrate.

Acknowledgements

The project was supported by “20 Policies about Colleges in Jinan” Program (Grant No: 2019GXRC047) and “migratory bird like” high level talent program in Tianqiao District.

References

[1] J. Guo, C. Shang, S. Yang, H. Guo, X. Wang, X. He, Materials & Design, 30(1), 129-134 (2009); https://doi.org/10.1016/j.matdes.2008.04.038

[2] N.K. Mishra, S.B. Mishra, R. Kumar, Surface and Coatings Technology, 260, 23-27 (2014); https://doi.org/10.1016/j.surfcoat.2014.07.089

[3] M. Nath, H.S. Tripathi, Ceramics International, 41(2), 3109-3115 (2015); https://doi.org/10.1016/j.ceramint.2014.10.155

[4] X. Wang, P. Ju, X. Lu, Y. Chen, F. Wang, Ceramics International, 48(3), 3615-3627 (2022); https://doi.org/10.1016/j.ceramint.2021.10.142

[5] V.P. Singh, A. Sil, R. Wear, 272(1), 149-158 (2011); https://doi.org/10.1016/j.wear.2011.08.004

[6] D. Chen, A. Huang, H. Gu, M. Zhang, Z. Shao, Ceramics International, 41(10), 14748-14753 (2015); https://doi.org/10.1016/j.ceramint.2015.07.202

[7] N.-n. Li, G.-l. Li, H.-d. Wang, J.-j. Kang, T.-s. Dong, H.-j. Wang, Materials & Design, 88, 906-914 (2015); https://doi.org/10.1016/j.matdes.2015.09.085

[8] K.V. Sreenivas Rao, G.C. Tejaswini, K.G. Girisha, Materials Today: Proceedings, 5(11), 24068-24074 (2018); https://doi.org/10.1016/j.matpr.2018.10.200

[9] A. Raj Sharma, R. Goyal, Materials Today: Proceedings, 48, 946-951 (2022); https://doi.org/10.1016/j.matpr.2021.05.677

[10] P. Zamani, Z. Valefi, K. Jafarzadeh, Ceramics International, 48(2), 1574-1588 (2022); https://doi.org/10.1016/j.ceramint.2021.09.237

[11] J. Chen, J. Xiao, Y. Zhang, Y. Wei, B. Han, Y. Li, S. Zhang, N. Li, Corrosion Science, 163, (2020); https://doi.org/10.1016/j.corsci.2019.108250

[12] D.W.L. B.K. Kim, and G.H. Ha, Journal of Thermal Spray Technology, 10(1), 133-137 (2001); https://doi.org/10.1361/105996301770349600

[13] P. Zamani, Z. Valefi, Surface and Coatings Technology, 316, 138-145 (2017); https://doi.org/10.1016/j.surfcoat.2017.03.022

[14] E. Abedi Esfahani, H. Salimijazi, M.A. Golozar, J. Mostaghimi, L. Pershin, Journal of Thermal Spray Technology, 21(6), 1195-1202 (2012); https://doi.org/10.1007/s11666-012-9810-x

[15] C. Haixiang, K. Dejun, Materials Chemistry and Physics, 251, (2020); https://doi.org/10.1016/j.matchemphys.2020.123200

[16] S.M. Hashemi, N. Parvin, Z. Valefi, M. Alishahi, Ceramics International, 45(17), 21108-21119 (2019); https://doi.org/10.1016/j.ceramint.2019.07.087

[17] J. Zhang, Z. Wang, P. Lin, W. Lu, Z. Zhou, S. Jiang, Journal of Thermal Spray Technology, 20(3), 508-513 (2010); https://doi.org/10.1007/s11666-010-9528-6